Journal of Catalysis 275 (2010) 202–210

Contents lists available at ScienceDirect

Journal of Catalysis

journal homepage: www.elsevier.com/locate/jcat

Influence of the nature of the precursor salts on the properties of Rh–Ge/TiO_2 catalysts for citral hydrogenation

Aurélie Vicente [a,b,*], Tchirioua Ekou [a,c], Gwendoline Lafaye [a], Catherine Especel [a], Patrice Marécot [a], Christopher T. Williams [d]

[a] Laboratoire de Catalyse en Chimie Organique, UMR 6503, Université de Poitiers, 40 avenue du Recteur Pineau, 86022 Poitiers Cedex, France
[b] Laboratoire Catalyse et Spectrochimie de Caen, EnsiCaen, Université de Caen, 6 boulevard Maréchal Juin, 14050 Caen Cedex, France
[c] Laboratoire de Thermodynamique et de Physico-Chimie du Milieu, Université d'Abobo-Adjame, 02 Bp 801 Abidjan 02, Ivory Coast
[d] Department of Chemical Engineering and NanoCenter, University of South Carolina, Columbia, SC 29208, United States

ARTICLE INFO

Article history:
Received 25 May 2010
Revised 15 July 2010
Accepted 15 July 2010
Available online 6 September 2010

Keywords:
Citral hydrogenation
Rhodium
Germanium
Titania
Bimetallic catalysts
FTIR of adsorbed CO

ABSTRACT

Four sets of Rh–Ge/TiO_2 bimetallic catalysts were prepared by surface redox reaction (i.e., catalytic reduction method) between hydrogen activated on a Rh parent catalyst and a Ge salt dissolved in aqueous solution. The four sets of catalysts differ depending on the presence or absence of chloride ions in the Rh and Ge precursor salts used (i.e., $RhCl_3$ vs. $Rh(NO_3)_3$, $GeCl_4$ vs. GeO_2). Samples were reduced either at a lower temperature (300 °C) or at a temperature chosen to induce a strong metal–support interaction (SMSI) effect (500 °C). Catalysts were characterized by elemental analysis, transmission electronic microscopy (TEM), and Fourier transform infrared (FTIR) spectroscopy of adsorbed CO and evaluated for their activity for the gas phase dehydrogenation of cyclohexane and selective hydrogenation of citral. Regardless of the nature of the Rh and Ge precursor salts, the catalytic reduction method causes the Ge to be in intimate contact with the Rh particles, favoring the citral hydrogenation toward unsaturated alcohols (UA: nerol and geraniol). For low Ge loadings, the bimetallic effect can be combined with the SMSI effect. It was observed that the UA selectivity is directly correlated to the ratio R ($R = \sum A(CO_{ads}$ on oxidized $Rh^{\geqslant 1+}$ species$)/\sum A(CO_{ads}$ on total exposed Rh species)) determined by FTIR. A better UA selectivity is obtained when bimetallic catalysts possess a surface in a predominantly oxidized state, a situation that is enhanced when chlorinated rhodium and germanium precursors are used.

1. Introduction

The selective hydrogenation of unsaturated α,β-aldehydes to the corresponding unsaturated alcohols is of considerable interest due to the numerous applications of those alcohols in fine chemistry. Particularly important is the selective hydrogenation of citral to unsaturated alcohols (UA: geraniol and nerol) employed in the production of flavors, fragrances, insect repellants, and in the synthesis of other compounds such as acetate and isobutyrate derivatives [1]. This is a challenging task, since the hydrogenation of the C=C bond is thermodynamically favored over the hydrogenation of the carbonyl group [2,3]. In general, catalysts based on noble metals show low activity and/or selectivity toward UA during the hydrogenation of unsaturated α,β-aldehydes. The activity and selectivity observed with these metals can be improved by interaction of the metallic phase with special supports [4–7], by formation of bimetallic compounds [8–15], or by combination of those two effects [16–18].

Recently, the hydrogenation of citral was performed over bimetallic Rh–Ge/TiO_2 and Pt–Ge/TiO_2 catalysts prepared by a surface redox reaction (namely the catalytic reduction method), in order to study the influence of the TiO_2-reducible support on the surface and catalytic properties of these such prepared catalysts [19]. We concluded that it is possible to combine a bimetallic effect with a reducible support (i.e., SMSI) effect for low germanium contents. Moreover, in contrast to alumina or a silica supports, the TiO_2 contributes to stabilization of the bimetallic particles prepared by catalytic reduction method.

The present contribution is the continuation of the study on Rh–Ge/TiO_2 catalysts prepared by catalytic reduction method, with the aim of determining the influence of the nature of the precursor salts for both Rh and Ge. In fact, several authors have observed a promoting effect of the chlorine for Pt/ZnO [6,20], as well as for Co supported on TiO_2, SiO_2, ZrO_2, Al_2O_3 [21] monometallic catalysts during the selective hydrogenation of unsaturated aldehydes (citral, cinnamaldehyde and especially crotonaldehyde). In this way, different Rh–Ge/TiO_2 catalysts were prepared from Rh and

* Corresponding author at: Laboratoire de Catalyse en Chimie Organique, UMR 6503, Université de Poitiers, 40 avenue du Recteur Pineau, 86022 Poitiers Cedex, France.
E-mail address: aurelie.vicente@ensicaen.fr (A. Vicente).

0021-9517/$ - see front matter © 2010 Elsevier Inc. All rights reserved.
doi:10.1016/j.jcat.2010.07.015

Ge precursor salts containing or not containing chloride ions. They were characterized by chemical analysis and transmission electron microscopy (TEM). Their catalytic performances were measured for cyclohexane dehydrogenation, which is a model, structure-insensitive reaction used to evaluate the interaction between Ge and the Rh active phase. The hydrogenating properties of these catalysts were evaluated for the selective hydrogenation of citral. Finally, the catalysts were characterized by FTIR of adsorbed CO in order to establish the relationship between the structure of the catalysts and the unsaturated alcohol selectivity.

2. Experimental

2.1. Catalyst preparation

The support used was a titania (Degussa P25, specific area = 50 $m^2\,g^{-1}$). It was calcined in flowing air for 4 h at 500 °C. Prior to its use, it was ground and then sieved to retain particles with sizes between 0.04 and 0.10 mm. Monometallic 1.0 wt%Rh/TiO_2 catalysts were prepared by impregnation using an aqueous solution of either $RhCl_3$ or $Rh(NO_3)_3$. The two corresponding catalysts are denoted in this manuscript as Rh_{Cl}/TiO_2 and Rh_N/TiO_2, respectively. Both catalysts were dried at 110 °C overnight, followed by calcination for 4 h in flowing air at 300 °C for Rh_{Cl} and at 500 °C for Rh_N. Finally, these two parent catalysts were reduced at 300 °C or 500 °C in flowing pure hydrogen for 4 h.

Bimetallic Rh–Ge/TiO_2 catalysts were prepared by catalytic reduction method, i.e., by surface redox reaction between hydrogen activated on Rh particles (from Rh_{Cl}/TiO_2 or Rh_N/TiO_2) and the Ge salt dissolved in water. Two different germanium salts were used: $GeCl_4$ in hydrochloric acid solution of pH = 1.0 (denoted Ge_{Cl}) or GeO_2 in ammonia medium of pH = 8.0 (denoted Ge_N). A measured amount of the prereduced parent catalyst (Rh_{Cl}/TiO_2 or Rh_N/TiO_2) was introduced into a reactor [22] under nitrogen and was activated at the same temperature as its first reduction, i.e., 300 °C or 500 °C, for 1 h under hydrogen. Then, the solution of the germanium precursor, previously degassed under hydrogen flow, was introduced onto the catalyst at room temperature. After 1-h reaction time under hydrogen bubbling, the solution was filtered out, and the catalyst was dried overnight at 100 °C. Finally, the bimetallic catalyst was reduced under hydrogen flow for 1 h at the same temperature as its parent catalyst (i.e., either at 300 °C or at 500 °C) using a 2 °C.min^{-1} heating rate). Blank rhodium catalysts were prepared following the same procedure but the germanium salt was replaced either by a hydrochloric solution of pH = 1.0 (denoted $blank_{Cl}$) or by an ammonia solution of pH = 8.0 (denoted $blank_N$). Finally, four Rh–Ge/TiO_2 bimetallic catalysts series were synthesized depending on the Rh and Ge precursor salts used: Rh_{Cl}–Ge_{Cl}/TiO_2, Rh_{Cl}–Ge_N/TiO_2, Rh_N–Ge_{Cl}/TiO_2, Rh_N–Ge_N/TiO_2. Likewise, four blank catalysts were prepared: Rh_{Cl} $blank_{Cl}/TiO_2$, Rh_{Cl} $blank_N/TiO_2$, Rh_N $blank_{Cl}/TiO_2$, and Rh_N $blank_N/TiO_2$.

The elemental analysis of the rhodium, germanium, and chlorine contents was determined by the "Service Central d'Analyse" of the CNRS. All the prepared catalysts are listed in Table 1 with their code name and metallic composition.

2.2. Transmission electron microscopy (TEM) measurements

Transmission electron microscopy (TEM) studies were performed on a Philips CM 120 instrument operating at 120 kV. All the samples were embedded in a polymeric resin (spurr) and cut into a section as small as 40 nm with an ultramicrotome equipped with a diamond knife. Cuts were then deposited on an Al grid previously covered with a thin layer of carbon. Average particle sizes were determined by measuring at least 100 particles for each sample analyzed, from at least five different micrographs.

Table 1
Characteristics of 1.0 wt% Rh monometallic and 1.0 wt% Rh–*x*wt%Ge bimetallic catalysts supported on TiO_2 (*x* = value of the amount of deposited Ge).

Catalyst/TiO_2	$T_{reduction}$ (°C)	wt% Cl	Average particle size (nm)
Rh_{Cl} parent	300	0.50	2.3
Rh_{Cl} $blank_{Cl}$	300	0.50	2.4
Rh_{Cl}–0.5Ge_{Cl}	300	0.50	2.5
Rh_{Cl}–1.0Ge_{Cl}	300	0.50	2.7
Rh_{Cl}–1.4Ge_{Cl}	300	0.50	2.7
Rh_{Cl}–1.6Ge_{Cl}	300	0.54	2.8
Rh_{Cl}–1.8Ge_{Cl}	300	0.54	2.8
Rh_{Cl} parent	500	⩽0.2	2.3
Rh_{Cl} $blank_{Cl}$	500	0.25	2.4
Rh_{Cl}–0.4Ge_{Cl}	500	⩽0.2	2.8
Rh_{Cl}–0.8Ge_{Cl}	500	⩽0.2	2.9
Rh_{Cl}–1.3Ge_{Cl}	500	⩽0.2	2.9
Rh_{Cl} $blank_N$	300	0.42	2.3
Rh_{Cl}–1.4Ge_N	300	0.50	2.6
Rh_{Cl} $blank_N$	500	⩽0.2	2.4
Rh_{Cl}–1.3Ge_N	500	⩽0.2	2.7
Rh_N parent	300	–	4.4
Rh_N $blank_{Cl}$	300	0.30	4.6
Rh_N–0.8Ge_{Cl}	300	0.30	4.9
Rh_N–1.2Ge_{Cl}	300	0.30	5.0
Rh_N–1.4Ge_{Cl}	300	0.33	5.0
Rh_N–1.8Ge_{Cl}	300	0.33	5.1
Rh_N parent	500	–	4.6
Rh_N $blank_{Cl}$	500	⩽0.2	4.9
Rh_N–0.7Ge_{Cl}	500	⩽0.2	5.1
Rh_N–1.2Ge_{Cl}	500	⩽0.2	5.2
Rh_N–1.4Ge_{Cl}	500	⩽0.2	5.2
Rh_N $blank_N$	300	–	4.6
Rh_N–0.7Ge_N	300	–	4.9
Rh_N–1.3Ge_N	300	–	4.9
Rh_N–1.6Ge_N	300	–	4.9
Rh_N $blank_N$	500	–	5.1
Rh_N–0.7Ge_N	500	–	4.9
Rh_N–1.4Ge_N	500	–	4.9
Rh_N–1.8Ge_N	500	–	5.0

2.3. Gas phase reaction

Cyclohexane dehydrogenation reaction was carried out under atmospheric pressure in a continuous flow reactor at 270 °C. Injection of cyclohexane was made using a calibrated motor-driven syringe. The partial pressures were 97 and 3 kPa for hydrogen and cyclohexane, respectively. All measurements were performed with a total flow rate of 100 mL min^{-1}. Analysis of the reaction products was performed by gas chromatography with a flame ionization detector (Varian 3400X) on a HP-PLOT Al_2O_3 "KCl" column. The only detected product was benzene.

2.4. Citral hydrogenation

The liquid phase hydrogenation of citral was carried out in a 300 mL stirred autoclave (Autoclave Engineers, fitted with a system for liquid sampling) at 70 °C and at constant pressure of 7 MPa. Prereduced catalysts (400 mg) were immersed into 90 mL of solvent (isopropanol 99%) without exposure to air before introduction into the autoclave. After a first flush with nitrogen and a second with hydrogen, the temperature was raised to 70 °C under 3 MPa of hydrogen. Then, a mixture of substrate (3 mL of citral) and isopropanol (10 mL) was loaded into the autoclave through a cylinder under a 7 MPa hydrogen pressure. Zero time was taken at this moment, and stirring was switched on.

Liquid samples were analyzed by gas chromatography on a Thermofinnigan chromatograph provided with a FID detector and capillary column DB-WAX (J&W, 30 m, 0.53 mm i.d.) using nitrogen as carrier gas.

2.5. Fourier transform infrared (FTIR) spectroscopy studies of adsorbed CO

Transmission FTIR spectra were collected in the single-beam mode, with a resolution of 2 cm^{-1}, using a Nicolet Nexus 470 FTIR spectrometer equipped with an MCT-B detector. A 10-cm-long stainless steel IR cell, with NaCl windows cooled by flowing water, was used to collect *in situ* spectra. A heating element wrapped around the cell allowed spectra collection at elevated temperatures. The cell temperature was monitored by a thermocouple placed in close proximity with the catalyst sample. Reference spectra of the clean surfaces in He were collected at room temperature. Difference spectra between the samples and the corresponding reference are shown in this paper. Catalyst samples were prepared as self-supported wafers with a diameter of 12 mm and a "thickness" of approximately 40 mg cm^{-2}.

Prior to CO adsorption experiments, all catalysts were reduced *in situ* for 2 h in flowing of H_2 at 300 °C or 500 °C. The flow rate during this, as well as all other subsequent treatments, was maintained at 70 mL min^{-1}. Following this reduction step, the samples were flushed with He at the same temperature and cooled in He to room temperature. At room temperature, a flowing 1% CO/He mixture (purified to remove trace amounts of O_2 and H_2O) was introduced into the cell and spectra were collected until steady state was reached. Helium was then purged through the cell to remove any weakly bonded CO. Spectral deconvolution was performed using the Galactic PeakSolve peak-fitting program.

3. Results and discussion

3.1. Characterization of catalysts

3.1.1. Deposition of Ge on Rh/TiO_2 catalysts

Fig. 1 shows the amount of germanium deposited on Rh_{Cl}/TiO_2 and Rh_N/TiO_2 catalysts reduced at 300 °C or 500 °C as a function of the germanium content initially introduced in solution. These results show that the amount of Ge deposited increases with the Ge content of the solution, regardless of reduction temperature and nature of Rh and Ge precursor salts used. It should be reminded that the preparation of bimetallic catalysts by the catalytic reduction method consists in depositing germanium by redox reaction between hydrogen activated over the rhodium surface and germanium ions. However, the deposition reaction may compete with the adsorption of the germanium salt on the titania support.

The comparison of the four bimetallic Rh–Ge/TiO_2 sets reduced at 300 °C or 500 °C (Fig. 1a and b) shows that for a same germanium content in the solution, the Ge deposition is higher for the Rh_{Cl}–Ge_{Cl} series, i.e., for the catalysts prepared from both chlorinated precursor salts ($RhCl_3$ and $GeCl_4$). Moreover, it appears that the amount of germanium deposited from the chlorinated precursor salt (Ge_{Cl}) is larger when Rh_X/TiO_2 samples (X = Cl or N) are reduced at 300 °C than at 500 °C, although the metallic particle size is independent of the reduction temperature for a given Rh_X–Ge_{Cl} catalyst (Table 1). This behavior may result from the SMSI effect induced by the titania support [5,17]. Effectively, through a combination of scanning transmission electron microscopy (STEM) and electron energy loss spectroscopy (EELS) experiments, Iddir et al. have evidenced the already reported geometrical relationship between group 8 metals and TiO_2 [23–25] and have given unambiguous proof of the SMSI phenomenon [26]. In fact, the Z-contrast imaging reveals a distortion of the reduced support around the metal clusters. These images show that the SMSI results from the tendency of reduced titania to encapsulate metal particles on its surface. In agreement with this work, the reduction of Rh_X/TiO_2 (X = Cl or N) catalysts at high temperature (500 °C) leads to the coverage of some fraction of the active Rh surface involving a lower germanium deposit on these samples.

Additionally, the Ge_{Cl} deposition is much smaller on the Rh_N/TiO_2 parent catalyst than on the Rh_{Cl}/TiO_2 one. This result is not surprising since the Rh_N/TiO_2 sample presents larger particles, which means less active sites for the catalytic reduction. In other hand, a lower Ge deposit on the support in the case of the Rh_N/TiO_2 catalyst can also contribute to this phenomenon.

3.1.2. Transmission electron microscopy measurements

The two monometallic Rh_{Cl}/TiO_2 and Rh_N/TiO_2 catalysts, selected bimetallic Rh–Ge/TiO_2 catalysts, and blank catalysts (prepared following the catalytic reduction procedure but without addition of the germanium salt) were characterized by TEM after reduction at 300 °C and 500 °C. Examples of characteristic images obtained for Rh_{Cl} $blank_{Cl}/TiO_2$ and Rh_N $blank_N/TiO_2$ reduced at 500 °C are shown in Fig. 2. Average particle sizes obtained through analysis of similar TEM images for all other considered samples are summarized in Table 1.

First, the comparable particle sizes suggest that the blank treatment does not lead to a sintering of the metal particles in the parent Rh_{Cl}/TiO_2 and Rh_N/TiO_2 for both the 300 °C and 500 °C reduction conditions. We have previously reported that Rh_{Cl}/TiO_2 catalysts are stable on titania support (contrary to silica or alumina) once immersed in an aqueous solution under hydrogen

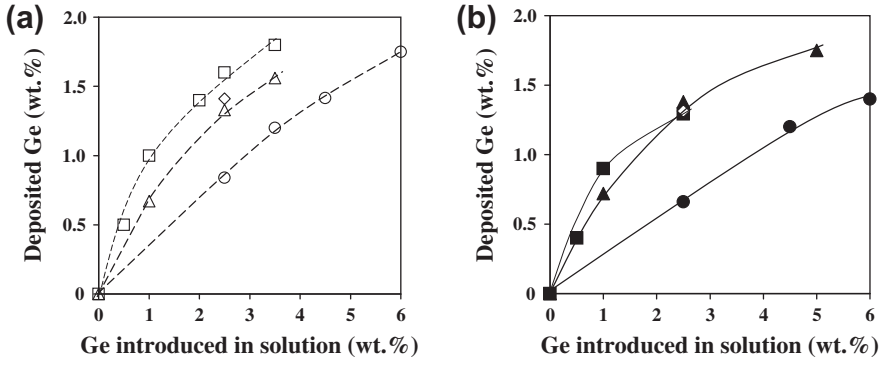

Fig. 1. Wt% Ge deposited by "catalytic reduction" as a function of the wt% Ge introduced in solution, for (□,■) Rh_{Cl}–Ge_{Cl}/TiO_2 catalysts, (△,▲) Rh_N–Ge_N/TiO_2 catalysts, (◇,◆) Rh_{Cl}–Ge_N/TiO_2 catalysts and (○,●) Rh_N–Ge_{Cl}/TiO_2 catalysts for (a) reduction at 300 °C and (b) reduction at 500 °C.

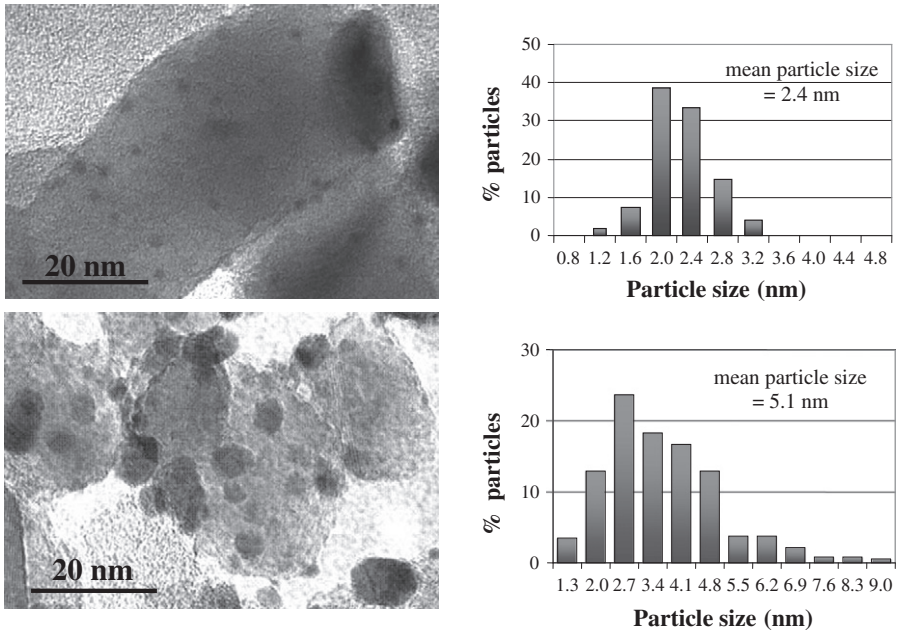

Fig. 2. TEM images and metal particle size distributions of: (a) Rh_{Cl} $blank_{Cl}/TiO_2$ and (b) Rh_N $blank_N/TiO_2$ catalysts reduced at 500 °C.

bubbling (catalytic reduction protocol) [27]. The present study suggests that TiO_2 is able to stabilize rhodium particles whatever the nature of the precursor salt used.

Moreover, the reduction temperature (300 °C or 500 °C) of a given monometallic or bimetallic catalyst has no effect on the particle size distribution and mean particle size (Table 1). Nevertheless, the average particle size of the bimetallic catalysts slightly increases with Ge addition, which is in accordance with a Ge deposition onto the parent metal particles.

The overall TEM results indicate that the Rh_N/TiO_2-based catalysts (monometallic, blank and bimetallic) present larger particle size distributions than the Rh_{Cl}/TiO_2-derived samples. They consequently present higher mean particle size (Table 1).

3.1.3. Catalytic activity for cyclohexane dehydrogenation

The different catalysts were tested for a structure-insensitive reaction [28–30], cyclohexane dehydrogenation, at 270 °C and at atmospheric pressure. The deposition of a catalytically inert metal (germanium) on rhodium would greatly affect the activity of the parent catalysts. This reaction would then permit to evaluate the interaction between germanium and the active phase after reduction.

3.1.3.1. Monometallic and blank catalysts. The data reported in Table 2 present the specific activity of parent and blank catalysts reduced at 300 °C and 500 °C. Concerning the samples reduced at 300 °C, the specific activity of the $blank_{Cl}$ and $blank_N/TiO_2$ is comparable to that of their corresponding parent catalysts (Rh_{Cl}/TiO_2 and Rh_N/TiO_2, respectively). This observation is in accordance with the TEM result that is the blank treatment of the monometallic Rh/TiO_2 catalysts does not lead to sintering of Rh particles.

However, the specific activity of the Rh_{Cl}/TiO_2 parent catalyst reduced at 300 °C increases when it is treated in ammonia solution (Rh_{Cl} $blank_N$). Conversely, the specific activity of the Rh_N/TiO_2 parent catalyst reduced at 300 °C decreases when it is treated in hydrochloric solution (Rh_N $blank_{Cl}$). These behaviors cannot be explained by a particle size effect. A poison effect of chlorine on the rhodium activity provides the best explanation for these observations on blank catalysts. This hypothesis was already proposed by Pieck and co-workers [31], who found a drop of platinum activity by introducing chlorine. It was proposed that neighboring adsorbed chlorine can modify the metal properties and lead to an alteration in the desorption of benzene, resulting in a decrease of the catalytic activity. Likewise, this poison effect of chlorine allows one to explain the high activity of the Rh_N parent catalyst compared to the Rh_{Cl}/TiO_2 one, even though its mean particle size is almost twice as large.

Table 2
Specific activity of parent and blank Rh/TiO_2 catalysts for cyclohexane dehydrogenation at 270 °C.

Catalyst/TiO_2	$T_{reduction}$ (°C)	Specific activity (mol h^{-1} g^{-1}_{metal})
Rh_{Cl} parent	300	4.7
Rh_{Cl} $blank_{Cl}$	300	4.7
Rh_{Cl} $blank_N$	300	5.9
Rh_N parent	300	6.4
Rh_N $blank_N$	300	5.8
Rh_N $blank_{Cl}$	300	4.9
Rh_{Cl} parent	500	3.1
Rh_{Cl} $blank_{Cl}$	500	2.3
Rh_{Cl} $blank_N$	500	2.8
Rh_N parent	500	5.2
Rh_N $blank_N$	500	3.0
Rh_N $blank_{Cl}$	500	1.7

The lower activities observed for the catalysts reduced at 500 °C instead of 300 °C are in accordance with the SMSI effect observed for TiO_2-supported catalysts reduced at high temperature. Indeed, the titania support is partially reduced during the reduction at 500 °C and then covers a portion of the active Rh surface.

3.1.3.2. Bimetallic catalysts. The evolution of the catalytic properties of the four bimetallic series reduced at 300 °C and 500 °C is shown in Fig. 3 as a function of the Ge content. The addition of germanium strongly inhibits the specific activity of rhodium whatever the Rh and Ge precursor salts and the reduction temperature of the catalysts. This result suggests significant interaction between the two metals, given that the average particle size is comparable within a given series (Table 1).

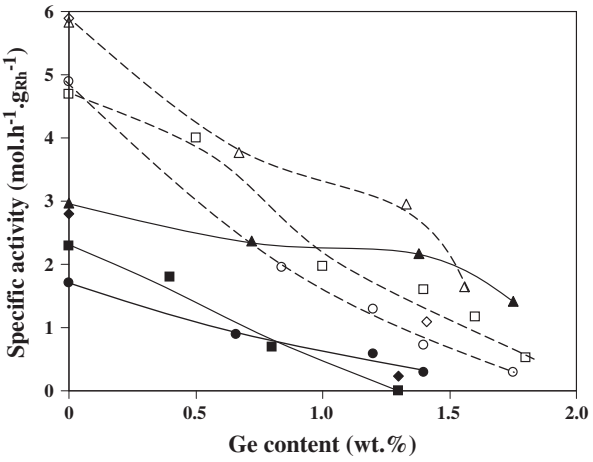

Fig. 3. Specific activity for cyclohexane dehydrogenation as a function of the wt% Ge deposited, for (□,■) Rh_{Cl}–Ge_{Cl}/TiO_2 catalysts, (△,▲) Rh_N–Ge_N/TiO_2 catalysts, (◇,◆) Rh_{Cl}–Ge_N/TiO_2 catalysts and (○,●) Rh_N–Ge_{Cl}/TiO_2 catalysts. Empty symbols are for reduction at 300 °C, while filled symbols are for reduction at 500 °C.

On the other hand, it appears that whatever the Ge loading and the nature of the precursor salts, the bimetallic catalysts reduced at 500 °C are less active than their counterparts reduced at 300 °C. This behavior results from the presence of $TiO_{(2-x)}$ ($x < 2$) species, which cover a part of the Rh surface after a reduction at 500 °C, as already noted for monometallic catalysts.

3.2. Citral hydrogenation

Fig. 4 presents the main reaction pathways that can occur during citral hydrogenation. The reduction of citral can lead to a variety of products. In this study, the main reaction products were found to be geraniol and nerol (unsaturated alcohols, UA), citronellal and citronellol. Side reactions can happen due to presence of chlorine in the precursor salt used. It has been reported in the literature that the presence of chlorine in the course of citral hydrogenation often leads to by-products (e.g., isopulegols) [32].

3.2.1. Monometallic and blank catalysts

The catalytic properties for citral hydrogenation of the Rh_{Cl}/TiO_2 and Rh_N/TiO_2 parent monometallic and corresponding Rh_{Cl} $blank_{Cl}$ and Rh_N $blank_N$ catalysts reduced at 300 °C and 500 °C are summarized in Table 3. For a given temperature, the Rh_{Cl}/TiO_2 parent catalyst is more active than the Rh_N/TiO_2 parent catalyst. The smaller particle size of the chlorinated samples supplies more accessible rhodium sites compared to the chlorine-free catalysts. The reduction at 500 °C compared to 300 °C induces a decrease in activity for the two parent catalysts. This is again explained by the presence of partially reduced support $TiO_{(2-x)}$ ($x < 2$) species created after reduction at high temperature, which can cover part of the metallic surface. Whatever the precursor salt, the SMSI effect is slightly beneficial to the selectivity toward the unsaturated alcohols. The beneficial effect of the SMSI phenomenon on the UA selectivity is known to be more important on Pt or Ir-based catalysts [16,17,33].

Table 3
Citral conversion after 60 min reaction time (between parentheses = after 20 min reaction time) and selectivity to unsaturated alcohols (UA) at 30% citral conversion on monometallic and blank Rh_{Cl} and Rh_N catalysts reduced at 300 °C and 500 °C.

Catalyst/TiO_2	$T_{reduction}$ (°C)	Citral conversion (%)	UA selectivity (%)
Rh_{Cl} parent	300	96 (80)	8
Rh_{Cl} $blank_{Cl}$	300	94	11
Rh_N parent	300	63	5
Rh_N $blank_N$	300	61	7
Rh_{Cl} parent	500	96 (65)	11
Rh_{Cl} $blank_{Cl}$	500	40	38
Rh_N parent	500	50	9
Rh_N $blank_N$	500	36	19

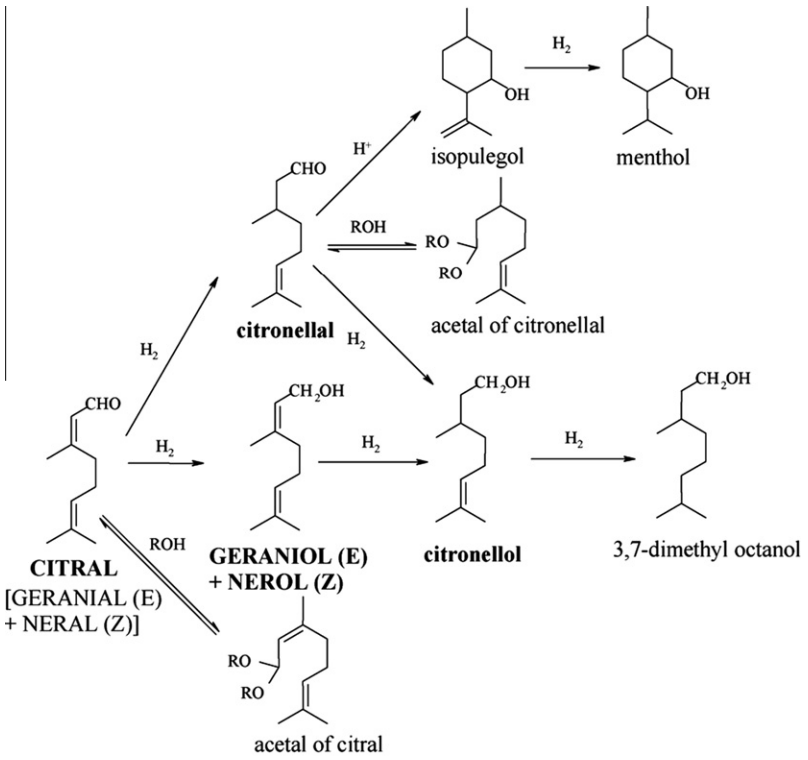

Fig. 4. Reaction scheme for citral hydrogenation.

Table 3 indicates that both Rh_{Cl} $blank_{Cl}$ and Rh_N $blank_N$ show the same performance as their parent monometallic counterparts. This result is in accordance with the TEM and cyclohexane dehydrogenation characterizations, showing similar characteristics for these respective samples. On the other hand, a decrease in the citral conversion (96% vs. 40% for Rh_{Cl} parent and Rh_{Cl} $blank_{Cl}$, respectively, and 50% vs. 36% for Rh_N ones) in parallel with an increase in the UA selectivity (11% vs. 38% and 9% vs. 19%, respectively) is observed between the parent and corresponding blank catalysts when they are reduced at 500 °C. This phenomenon cannot be explained by a particle size effect, since the sizes of the particles for the catalysts reduced at 500 °C are comparable. Thus, the higher UA selectivity, as well as the drop of citral hydrogenation activity, of the Rh_{Cl} $blank_{Cl}$ and Rh_N $blank_N$ could be explained by the presence of more $TiO_{(2-x)}$ moieties in comparison with their respective Rh_{Cl} and Rh_N parent catalysts. Indeed, we have demonstrated in previous work that the immersion of Rh parent catalysts, reduced at 500 °C, in an aqueous medium (e.g., such as the blank treatment) partially destroyed the $TiO_{(2-x)}$ species (i.e., decreased the SMSI effect). The remaining part on the resulting blank catalyst is then added to the $TiO_{(2-x)}$ moieties formed during the subsequent reduction at 500 °C [19,27].

3.2.2. Bimetallic catalysts

In order to study the influence of the nature of metallic precursor salt on the hydrogenating properties, the monometallic Rh_{Cl}/TiO_2 and Rh_N/TiO_2 catalysts reduced at 300 °C and 500 °C were modified by addition of various amount of germanium introduced from $GeCl_4$ (Ge_{Cl}) or GeO_2 (Ge_N) precursor. Each bimetallic sample was reduced under hydrogen at the temperature applied to the monometallic parent (300 °C or 500 °C).

Fig. 5a displays the citral conversion after 60-min reaction time of bimetallic Rh_x–Ge_y/TiO_2 catalysts (x and y = Cl or N) as a function of the germanium content. For each series, the value reported for wt%Ge equal to zero refers to that of the corresponding blank sample.

For the four sets of catalysts reduced at 300 °C, the citral conversion decreases with the germanium content, and the most loaded germanium samples present the lowest hydrogenating activities. In the 1.0–1.5 wt% Ge range, bimetallic catalysts prepared with both chlorinated precursors (Rh_{Cl}–Ge_{Cl}/TiO_2) are the most active (conversion of 60% at 60 min), followed by Rh_N–Ge_{Cl}/TiO_2 (conversion = 45%), Rh_N–Ge_N/TiO_2 (conversion = 30%) and finally Rh_{Cl}–Ge_N/TiO_2 with only 10% of conversion. The different activities in citral hydrogenation observed for Rh_{Cl}- and Rh_N-based catalysts could be explained by the fact that the Rh_N/TiO_2-based catalysts (blank and bimetallic) present bigger particle size (around 4.6 nm for Rh_N–Ge_N/TiO_2 and Rh_N–Ge_{Cl}/TiO_2) than the Rh_{Cl}/TiO_2-derived samples (around 2.8 nm for Rh_{Cl}–Ge_{Cl}/TiO_2 and Rh_{Cl}–Ge_N/TiO_2) (Table 1). On the other hand, the differences of activity between two bimetallic catalysts prepared from the same Rh_{Cl} or Rh_N parent catalyst (especially Rh_{Cl}–Ge_{Cl}/TiO_2 and Rh_{Cl}–Ge_N/TiO_2) are not due to an effect of particle size, but certainly to an effect of the nature of the germanium precursor salt. Thus, it appears that the rhodium activity is less inhibited by germanium deposit from $GeCl_4$ than from GeO_2 precursor.

After reduction at 500 °C, a decrease in the activities is observed for all the samples compared to their counterparts reduced at 300 °C. This phenomenon does not result from a variation of the metal particle sizes, since the TEM study showed comparable sizes for catalysts reduced at 300 °C and 500 °C (Table 1). This behavior results from the presence of $TiO_{(2-x)}$ species, which cover a part of the Rh surface after a reduction at 500 °C (i.e., SMSI effect). In addition, a change of the germanium reduction state in the vicinity of the rhodium during reduction at 500 °C could also induce this phenomenon.

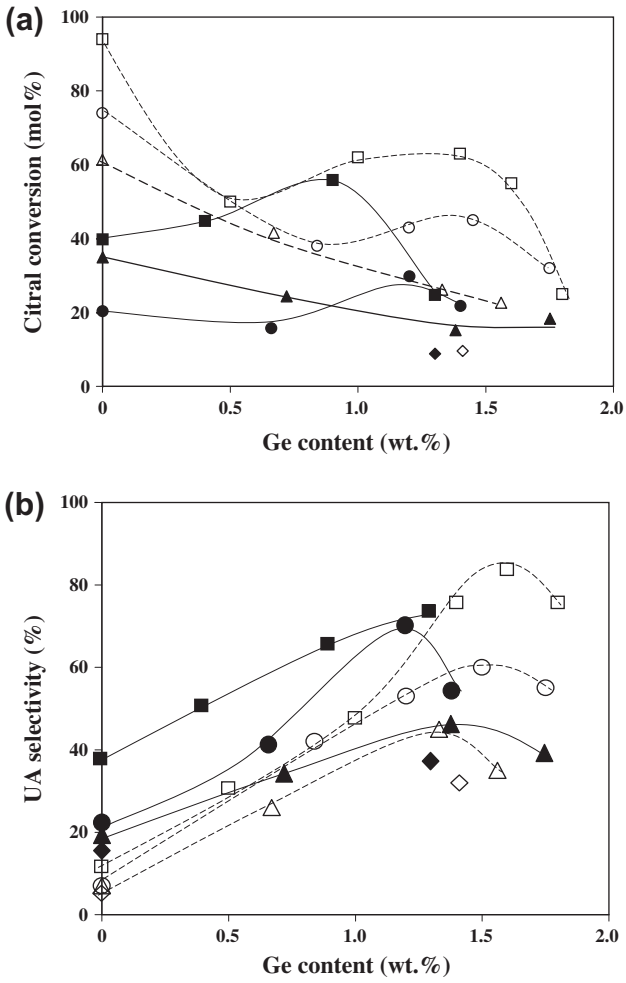

Fig. 5. (a) Citral conversion after 60-min reaction time and (b) unsaturated alcohols selectivity at 30% citral conversion as a function of Ge content for Rh–Ge/TiO_2 bimetallic catalysts: (□,■) Rh_{Cl}–Ge_{Cl} catalysts, (△,▲) Rh_N–Ge_N catalysts, (◇,◆) Rh_{Cl}–Ge_N catalysts and (○,●) Rh_N–Ge_{Cl} catalysts. Empty symbols are for reduction at 300 °C, while filled symbols are for reduction at 500 °C.

Finally, regarding to the conversion results, Rh_{Cl}–Ge_{Cl}/TiO_2 catalysts are the most active in the 1.0–1.5wt% Ge range after reduction at 300 °C and at lower Ge content (⩽1.0 wt%) after reduction at 500 °C.

The comparison of the UA selectivities obtained for all the bimetallic systems after reduction at 300 °C and 500 °C is given in Fig. 5b. The curves show that the UA selectivity displays a maximum as a function of the germanium loading. The decrease in the UA selectivity for the highest Ge contents is due to an increase in the by-products formation.

Ge deposition by catalytic reduction promotes the selective hydrogenation of the C=O bond and the formation of unsaturated alcohols. Nevertheless, the UA selectivity is strongly dependent on the precursor salt nature. In fact, after reduction at 300 °C, for Ge contents ⩽1 wt% the two sets of catalysts Rh_{Cl}–Ge_{Cl}/TiO_2 and Rh_N–Ge_{Cl}/TiO_2 present similar selectivities. For higher Ge contents, a strong increase in the UA selectivity appears only for the Rh_{Cl}–Ge_{Cl}/TiO_2 system (85% of UA selectivity vs. 65% for Rh_N–1.4 wt%Ge_{Cl}/TiO_2) while the Rh_N–Ge_N/TiO_2 and Rh_{Cl}–Ge_N/TiO_2 series do not exceed 40%. For the four sets of catalysts reduced at 500 °C, there was generally an increase in the UA selectivity, especially at low Ge contents. It is known that the reducible support treated at high temperature can participate to the activation of the C=O bond [19,33–35]. Thus, the present results show that

it is possible to combine the bimetallic effect (interaction between Ge and Rh) with the SMSI effect (formation of $TiO_{(2-x)}$ ($x < 2$) species) whatever the nature of the precursor salts. However, it seems necessary to use chlorinated germanium salt to favor the C=O bond hydrogenation, with the best results obtained when deposited on the parent catalyst derived from chlorinated rhodium salt.

3.3. FTIR of chemisorbed CO

Deconvoluted FTIR spectra of CO adsorbed at room temperature on the Rh_{Cl}–$blank_{Cl}/TiO_2$ and bimetallic Rh_{Cl}–$x$wt%Ge_{Cl}/TiO_2 samples reduced at 300 °C are shown in Fig. 6. Preliminary FTIR investigations showed that Ge/TiO_2 does not adsorb CO molecules. Six different features are present on the spectra, located around 2120 cm^{-1}, 2095 cm^{-1}, 2070 cm^{-1}, 2030 cm^{-1}, 1990 cm^{-1}, and 1860 cm^{-1}. The corresponding peak assignments are summarized in Table 4. Previous results on the adsorption of CO on Rh/TiO_2 allowed us to assign the various peaks to the symmetric and antisymmetric stretching vibrations of a geminal dicarbonyl species and to the linear- and bridge-bonded CO stretching vibrations on different Rh sites [36,37].

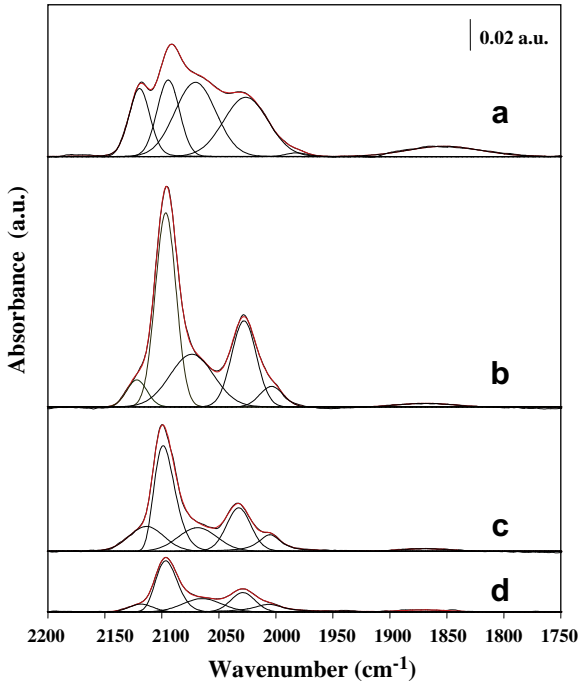

Fig. 6. FTIR spectra of adsorbed CO at room temperature on the (a) Rh_{Cl} $blank_{Cl}/TiO_2$, (b) Rh_{Cl}–$1.0Ge_{Cl}/TiO_2$, (c) Rh_{Cl}–$1.6Ge_{Cl}/TiO_2$ and (d) Rh_{Cl}–$1.8Ge_{Cl}/TiO_2$ samples reduced at 300 °C.

For the Rh_{Cl}–$blank_{Cl}/TiO_2$ monometallic catalyst, the presence of germinal dicarbonyl species on Rh^{1+} sites (symmetric and antisymmetric stretches at 2095 and 2030 cm^{-1}, respectively) can be attributed to the presence of small isolated Rh particles and/or oxidation of Rh^0 by isolated-OH groups from the support [38–40]. The spectral features at around 2070 and 1860 cm^{-1} can be assigned, respectively, to linear- and bridge-bonded CO adsorbed on Rh^0 atoms, and the peak revealed near 1990 cm^{-1} corresponds to bridge-bonded CO species on Rh^{1+} sites. Finally, the peak at 2120 cm^{-1} observed for Rh catalysts supported on TiO_2 is generally attributed to linear-bonded CO on higher oxidation state rhodium sites, such as Rh^{2+} and/or Rh^{3+}.

In the case of the bimetallic Rh_{Cl}–Ge_{Cl}/TiO_2 samples, Fig. 6 shows that the total surface of adsorbed CO decreases progressively with the increase in the germanium content. Since TEM characterization showed a comparable mean particle size between the bimetallic Rh_{Cl}–Ge_{Cl} catalysts and the Rh_{Cl}–$blank_{Cl}$ one (Table 1), it suggests that Ge gradually covers the Rh surface. In fact, the evolution of the spectral features with the Ge content is comparable with previous results obtained with bimetallic Rh–Ge supported on alumina [41]. Indeed, Table 4 indicates that the different surface CO species are not affected proportionally by the presence of Ge. The geminal dicarbonyl species adsorbed on Rh^{+1} are present on all bimetallic samples, with the symmetric peak having a higher intensity in these cases. Furthermore, the species assigned to Rh^0 (bridged and linearly bonded species) decrease with the Ge content of the samples. The peak corresponding to bridge-bonded CO species on Rh^0 disappears from the spectra of the sample with the highest germanium content (Rh_{Cl}–$1.8Ge_{Cl}$). These observations suggest that the presence of Ge leads to a better dispersion of rhodium in the form of Rh^{+1} and the creation of smaller Rh ensembles at the expense of the larger Rh^0 surfaces.

A relationship is known in the literature between the ratio of the relative intensities of the two geminal bonds and the angle α formed between the two adsorbed CO molecules on the same Rh^{1+} site [42]:

Table 4
Peak assignments (cm^{-1}) and relative surface areas (%) under each peak observed during the adsorption of CO on TiO_2-supported Rh blank and Rh–Ge bimetallic samples reduced at 300 °C.

Catalyst /TiO_2	Linear on $Rh^{>1+}$ ORhCO	Gem sym on Rh^{1+} $Rh(CO)_2$	Linear on Rh^0 RhCO	Gem asym on $Rh^{1+}Rh(CO)_2$	Bridge on Rh^{1+}	Bridge on Rh^0	$\frac{I_{sym}}{I_{asym}}$	R^*
Rh_{Cl} $blank_{Cl}$	**2120**	**2094**	**2071**	**2026**	**1982**	**1853**	0.7	0.61
	15.3%	*17.7%*	*31.3%*	*27.2%*	*0.7%*	*7.8%*		
Rh_{Cl}–$1.0Ge_{Cl}$	**2122**	**2097**	**2074**	**2028**	**2004**	**1869**	1.9	0.74
	5.6%	*41.6%*	*23.8%*	*22.0%*	*5.0%*	*1.9%*		
Rh_{Cl}–$1.6Ge_{Cl}$	**2127**	**2099**	**2077**	**2033**	**2005**	**1869**	2.1	0.82
	15.3%	*39.0%*	*16.1%*	*19.1%*	*8.6%*	*1.9%*		
Rh_{Cl}–$1.8Ge_{Cl}$	**2118**	**2097**	**2065**	**2029**	**2006**	–	2.4	0.80
	7.0%	*42.9%*	*19.9%*	*18.0%*	*12.2%*			
Rh_N $blank_N$	–	**2104**	**2086**	**2022**	**1987**	–	–	0.68
		41.5%	*32.2%*	*25.9%*	*0.4%*			
Rh_N–$1.3Ge_N$	**2118**	**2099**	**2071**	**2032**	**2010**	**1885**	–	0.71
	6.9%	*35.0%*	*23.3%*	*19.5%*	*9.5%*	*5.7%*		
Rh_N–$1.2Ge_{Cl}$	**2124**	**2097**	**2076**	**2029**	**2015**	–	–	0.78
	5.1%	*42.3%*	*22.2%*	*23.8%*	*6.6%*			
Rh_{Cl}–$1.4Ge_N$	**2119**	**2100**	**2069**	**2034**	**2014**	–	–	0.69
	7.2%	*33.6%*	*30.7%*	*17.4%*	*11.0%*			

* $R = \sum A(CO_{ads}$ on oxidized $Rh^{\geq 1+}$ species$)/\sum A(CO_{ads}$ on total exposed Rh species$)$.

$$I_{\text{symmetric}}/I_{\text{antisymmetric}} = \text{cotan}(\alpha)$$

Thus, the rise of this ratio with Ge content (reported in Table 4) for the Rh_{Cl}–Ge_{Cl}/TiO_2 set indicates that the angle between the geminally adsorbed CO molecules decreases upon increasing Ge content. This is consistent with an increase in the Ge quantity in close vicinity with Rh atoms.

Table 4 gives also a comparison between the FTIR results of adsorbed CO on bimetallic samples, with comparable Ge content, from the Rh_N–Ge_N, Rh_N–Ge_{Cl} and Rh_{Cl}–Ge_N series. For all the samples, a predominance of the symmetric geminal dicarbonyl species is observed, followed by the linear Rh^0 and antisymmetric geminal dicarbonyl species. A ratio labeled *R* was calculated as indicated below in order to examine the effect of the nature of the metallic precursor salts on the surface properties of Rh–Ge catalysts.

$$R = \sum A(\text{CO}_{\text{ads}} \text{ on oxidized } \text{Rh}^{\geq 1+} \text{ species}) / \sum A(\text{CO}_{\text{ads}} \text{ on total exposed Rh species})$$

with A = infrared band Areas.

This ratio represents the proportion of CO molecules adsorbed on oxidized and reduced Rh species in each catalyst (Table 4).

In Fig. 7, the evolution of the unsaturated alcohol selectivity, obtained during citral hydrogenation, is represented as a function of the R ratio for all the samples (Rh blank and Rh–Ge/TiO_2 catalysts) characterized by FTIR. The UA selectivity evolves linearly with the R ratio, which suggests that UA selectivity is promoted by two simultaneous phenomena: (1) the presence of oxidized rhodium species, generated by the addition of germanium, and (2) the preferential deposit of Ge on the Rh^0 species, these last ones being probably the main sites responsible for the C=C hydrogenation of citral. The increase in the presence of $Rh^{\geq 1+}$ species for the bimetallic catalysts suggests a charge transfer from Rh to Ge favorable to the activation of the C=O bond of citral.

Finally, for comparable Ge loadings, the highest R ratio is obtained when the combination Cl–Cl is used in the preparation of the catalyst. Consequently, chlorine in close contact with Rh and Ge seems to be a determining parameter to selectively control the reaction of citral hydrogenation toward the formation of unsaturated alcohols.

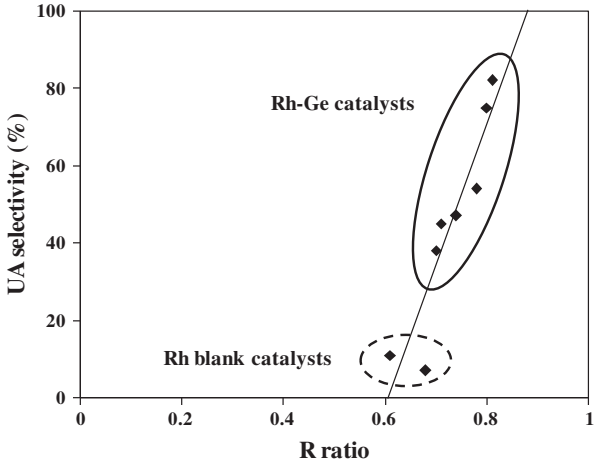

Fig. 7. Unsaturated alcohols selectivity as a function of *R* ($R = \Sigma A(CO_{ads}$ on $Rh^{\geq 1+}$ species)/$\Sigma A(CO_{ads}$ on total exposed Rh species)).

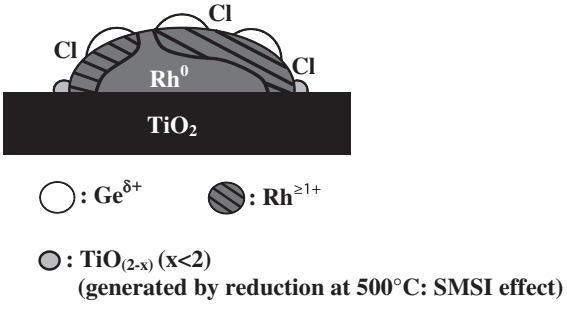

Fig. 8. Scheme of a highly selective Rh–Ge/TiO_2 particle toward the unsaturated alcohols during citral hydrogenation.

4. Conclusions

Four series of Rh–Ge/TiO_2 bimetallic catalysts prepared by catalytic reduction method from different precursor salts either containing or not containing chlorine were studied: Rh_{Cl}–Ge_{Cl}, Rh_{Cl}–Ge_N, Rh_N–Ge_{Cl}, and Rh_N–Ge_N. For the two reduction temperatures studied (300 °C or 500 °C), the use of a chlorinated rhodium precursor results in particle size around 2.3 nm, while samples from a nitrate precursor present larger particle size around 4.6 nm.

Whatever the precursor salt used, the germanium deposited on the parent catalyst by catalytic reduction method increases with the germanium amount introduced in solution. The protocol used for the preparation of the Rh–Ge/TiO_2 catalysts (immersion of the parent sample in either aqueous HCl or NH_3 solutions under H_2 bubbling) does not cause modification of the particle size of the corresponding parent catalyst. Thus, the drop of activity observed for all the Rh–Ge catalyst series for cyclohexane dehydrogenation reveals a strong interaction between the two metals.

The addition of germanium to rhodium promotes UA selectivity during the citral hydrogenation. This promoting effect strongly depends on the precursor salt nature. Indeed, FTIR investigation of adsorbed CO reveals that the proportion of $Rh^{\geq 1+}$ and Rh^0 species on the catalyst surface depends on the nature of the precursor salt used. The Rh^0 sites are responsible for C=C hydrogenation of citral while the $Rh^{\geq 1+}$ sites would activated the C=O bond. It is then necessary to strongly deactivate the Rh^0 sites by addition of Ge or by reduction of the TiO_2-supported catalysts at high temperature (500 °C – SMSI effect) to promote the reaction toward the formation of unsaturated alcohols. Moreover, partially oxidized Ge and $TiO_{(2-x)}$ species reduced at 500 °C participate also to the activation of the C=O bond. For low Ge loadings, these two effects can be combined.

Thus, the most selective bimetallic catalysts possess a surface in a predominantly oxidized state, a situation that is enhanced when chlorinated precursors are used for both rhodium and germanium. This result allows us to propose a scheme in Fig. 8 of a highly selective Rh–Ge/TiO_2 particle.

References

[1] Kirk-Othmer, in: I. Kroschwitz (Ed.), Encyclopedia of Chemical Technology, fourth ed., vol. 6, John Wiley & Sons, New York, 1992.
[2] P. Gallezot, D. Richard, Catal. Rev. Sci. Eng. 40 (1998) 81.
[3] P. Mäki-Arvela, J. Hájek, T. Salmi, D.Yu. Murzin, Appl. Catal. A 292 (2005) 1.
[4] M.A. Vannice, B. Sen, J. Catal. 115 (1989) 65.
[5] A.B. Da Silva, E. Jordão, M.J. Mendes, P. Fouilloux, Appl. Catal. A 148 (1997) 253.
[6] A. Sepúlveda-Escribano, F. Coloma, F. Rodríguez-Reinoso, J. Catal. 178 (1998) 649.
[7] M. Consonni, D. Jokic, D. Yu Murzin, R. Touroude, J. Catal. 188 (1999) 165.
[8] A. Giroir-Fendler, D. Richard, P. Gallezot, Catal. Lett. 5 (1990) 175.
[9] M. Boutonnet Kizling, C. Bigey, R. Touroude, Appl. Catal. A 135 (1996) L13.
[10] M. Abid, R. Touroude, Catal. Lett. 69 (2000) 139.
[11] G. Lafaye, T. Ekou, C. Micheaud-Especel, C. Montassier, P. Marécot, Appl. Catal. A 257 (2004) 107.
[12] B. Didillon, A. El Mansour, J.P. Candy, J.P. Bournonville, J.M. Basset, Stud. Surf. Sci. Catal. 59 (1991) 137.
[13] B. Didillon, J.P. Candy, F. Le Peletier, O.A. Ferretti, J.M. Basset, Stud. Surf. Sci. Catal. 78 (1993) 147.
[14] J.N. Coupé, E. Jordão, M.A. Fraga, M.J. Mendes, Appl. Catal. A 199 (2000) 45.

[15] R. Liu, Y. Yu, K. Yoshida, G. Li, H. Jiang, M. Zhang, F. Zhao, S. Fujita, M. Arai, J. Catal. 269 (2010) 191.
[16] P. Reyes, H. Rojas, G. Pecchi, J.L.G. Fierro, J. Mol. Catal. A 179 (2002) 293.
[17] P. Reyes, H. Rojas, J.L.G. Fierro, J. Mol. Catal. A 203 (2003) 203.
[18] A.M. Silva, O.A.A. Santos, M.J. Mendes, E. Jordão, M.A. Fraga, Appl. Catal. A 241 (2003) 155.
[19] T. Ekou, A. Vicente, G. Lafaye, C. Especel, P. Marecot, Appl. Catal. A 314 (2006) 73.
[20] F. Ammari, J. Lamotte, R. Touroude, J. Catal. 221 (2004) 32.
[21] Y. Nitta, Y. Hiramatsu, T. Imanaka, J. Catal. 126 (1990) 235.
[22] J.M. Dumas, C. Geron, H. Hadrane, P. Marecot, J. Barbier, J. Mol. Catal. 77 (1992) 87.
[23] S.J. Tauster, S.C. Fung, R.L.J. Garten, J. Am. Chem. Soc. 100 (1978) 170.
[24] R. Burch, Appl. Catal. 12 (1984) 285.
[25] G.L. Haller, D.E. Resasco, Adv. Catal. 36 (1989) 173.
[26] H. Iddir, M.M. Disko, S. Ogut, N.D. Browning, Micron 36 (2005) 233.
[27] T. Ekou, A. Vicente, G. Lafaye, C. Especel, P. Marecot, Appl. Catal. A 314 (2006) 64.
[28] J.A. Cusumano, G.W. Dembinski, J.H. Sinfeld, J. Catal. 5 (1966) 458.
[29] D.W. Blakely, G.A. Somorjai, J. Catal. 42 (1976) 458.
[30] I. Rodriguez-Ramos, A. Guerrero-Ruiz, J. Catal. 135 (1992) 458.
[31] C.L. Pieck, P. Marecot, J.M. Parera, J. Barbier, Appl. Catal. A 126 (1995) 153.
[32] P. Mäki-Arvela, L.P. Tiainen, A.K. Neyestanaki, R. Sjöholm, T.K. Rantakylä, E. Laine, T. Salmi, D.Yu. Murzin, Appl. Catal. A 237 (2002) 181.
[33] U.K. Singh, M.A. Vannice, Stud. Surf. Sci. Catal. 130 (2000) 497.
[34] M. Englisch, A. Jentys, J.A. Lercher, J. Catal. 166 (1997) 25.
[35] A. Huidobro, A. Sepúlveda-Escribano, F. Rodríguez-Reinoso, J. Catal. 212 (2002) 94.
[36] S. Trautmann, M. Baerns, J. Catal. 150 (1994) 335.
[37] Z.L. Zhang, A. Kladi, X.E. Verykios, J. Mol. Catal. 86 (1994) 229.
[38] P. Basu, D. Panayotov, J.T. Yates Jr, J. Am. Chem. Soc. 110 (1988) 2074.
[39] F. Solymosi, M. Pasztor, J. Phys. Chem. 89 (1985) 4789.
[40] S.S.C. Chuang, S. Debnath, J. Mol. Catal. 79 (1993) 323.
[41] G. Lafaye, C. Mihut, C. Especel, P. Marécot, M. Amiridis, Langmuir 20 (24) (2004) 10612.
[42] F.A. Cotton, G. Wilkinson, third ed., Interscience Publishers, New York, 1972.